J Solid State Electrochem (2007) 11:1077–1084
DOI 10.1007/s10008-006-0241-9

ORIGINAL PAPER

Interfacial properties of self-organized TiO_2 nanotubes studied by impedance spectroscopy

A. G. Muñoz · Q. Chen · P. Schmuki

Received: 15 September 2006 / Revised: 19 October 2006 / Accepted: 3 November 2006 / Published online: 25 November 2006
© Springer-Verlag 2006

Abstract The semiconductor properties of the interface TiO_2/electrolyte in high organized porous oxide structures were analyzed by means of impedance spectroscopy near the flat band potential. The impedance and capacitance studies performed on the as-anodized and thermally treated samples (anatase) indicate the presence of a duplex structure formed by (1) the oxide at the bottom of the pores and (2) the walls of pores with different donor densities and surface state concentrations.

Keywords TiO_2 nanotubes · Impedance spectroscopy · A-semiconductors

Introduction

Due to its semiconducting and photoelectrochemical properties [1], the anodic formation of uniform and compact layers of TiO_2 in different electrolytes was extensively investigated [2–4]. However, it is only in recent years that the interest in anodic TiO_2 layers has been renewed due to reports on ordered formation of porous TiO_2. The major part of TiO_2 applications is based on its photocatalytic and photoelectrochemical properties, which mostly are surface area controlled. Therefore, various methods to generate nanoporous titanium oxide with a high specific area were developed, using mainly sintering processes of nanoparticles obtained by sol–gel procedures. The surface properties of these porous materials can be further modified and improved by annealing [5–7], doping with nitrogen [8] or carbon [9], or by attaching suitable organic dyes, the latter being a common procedure for optimizing the operation of solar cells [1, 10, 11]. Recently, the formation of highly organized porous layers of TiO_2 by anodization in F^- containing electrolytes was investigated and optimized with a great success [12–16]. This fact allowed extending the potential of this material for technological applications not only due to the highly organized structure but also due to the good electrical contact with the substrate, which presents some advantages in an attempt to introduce more simple assemblies, for example, in the construction of photochromic devices. Therefore, a better understanding of the semiconductor properties of such self-organized porous oxide structures is essential for numerous applications involving chemical, electrochemical, and photoelectrochemical processes at the semiconductor/electrolyte interface.

In this paper, we analyze the impedance behavior of layers of high ordered TiO_2 nanotubes formed by anodization to gain more insight into the surface electronic properties in these structures.

A. G. Muñoz · Q. Chen · P. Schmuki
Department of Materials Science,
University of Erlangen-Nürnberg,
91058 Erlangen, Germany

Present address:
A. G. Muñoz (✉)
Institut für Angewandte Physik,
Heinrich-Heine-Universität Düsseldorf,
Universitätsstraße 1,
40225 Düsseldorf, Germany
e-mail: andres.munoz@uni-duesseldorf.de

Experimental details

Sheets of Ti (9.6% purity) were used as working electrode. They were first mechanically mirror polished with emery paper and diamond suspension and then sonicated in acetone, isopropanol, and methanol followed by drying

with a nitrogen stream. The anodization and electrochemical characterization were performed in a classical cell with a three-electrode arrangement with nondeareated solutions. A Pt sheet and a $Hg/Hg_2SO_4/K_2SO_4$(sat) system were used as a counter and reference electrode, respectively. In a similar way as reported in [17], the anodization of samples consisted of a potential ramp of 500 mV s^{-1} from the open circuit potential up to different $U\tau$, followed by a potential holding at this value for a time (τ). In this way, three types of oxide layers were generated:

(1) compact layers in 1 M H_3PO_4 ($U\tau$=10 V, τ=10 min, oxide thickness ca. 25 nm),
(2) layers of short tubes in 1 M H_3PO_4+0.3% HF ($U\tau$= 10 V, τ=2 h, thickness ca. 500 nm),
(3) layers of long tubes in 1 M NaH_2PO_4+0.5% HF ($U\tau$= 20 V, τ=2 h, thickness ca. 1 μm).

This treatment was performed by means of a high-voltage potentiostat Jaissle IMP 88. Subsequent thermal annealing of oxide layers was carried out at 450 °C in air during 3 h using a heating and cooling rate of 20 °C/s to convert the amorphous oxide in anatase. Figure 1 shows the morphologies of the porous structures where different pore geometries are observed, namely, short pores of 75 nm of diameter (method 2) and long pores with an aperture of 150 nm (method 3). The thickness of the pore walls is difficult to be determined by scanning electron microscopy (SEM), but it can be estimated to be between 20 and 30 nm.

The electrochemical characterization was performed in acetate buffer solution of pH 6. Acetate and borate buffer solutions of pH 2.73–9 were also used for pH-dependence studies. All measurements were performed in the dark.

The surface morphology of nanostructured layers was characterized by means of a scanning electron microscope Hitachi SEM FE 4800.

Impedance measurements were carried out with a universal electrochemical interface and an impedance spectrum analyzer Zahner IM6d.

Results and discussion

Impedance studies

The analysis of the impedance spectroscopy performed on the oxide layers offers a first approach to investigate their electronic properties. Spectra were taken at potentials more positive than and close to the flat band potential to avoid modifying the conductive properties arising from the reduction to Ti^{3+} [18].

Figure 2a shows the impedance spectra taken at different potentials on amorphous and annealed samples of compact and porous oxides constituted by ordered tubes of 0.5 and 1 μm. At first glance, the impedance spectra denote the presence of two time constants, which can be ascribed to the response of the semiconductor space charge layer in series with the Helmholtz layer in the electrolyte side.

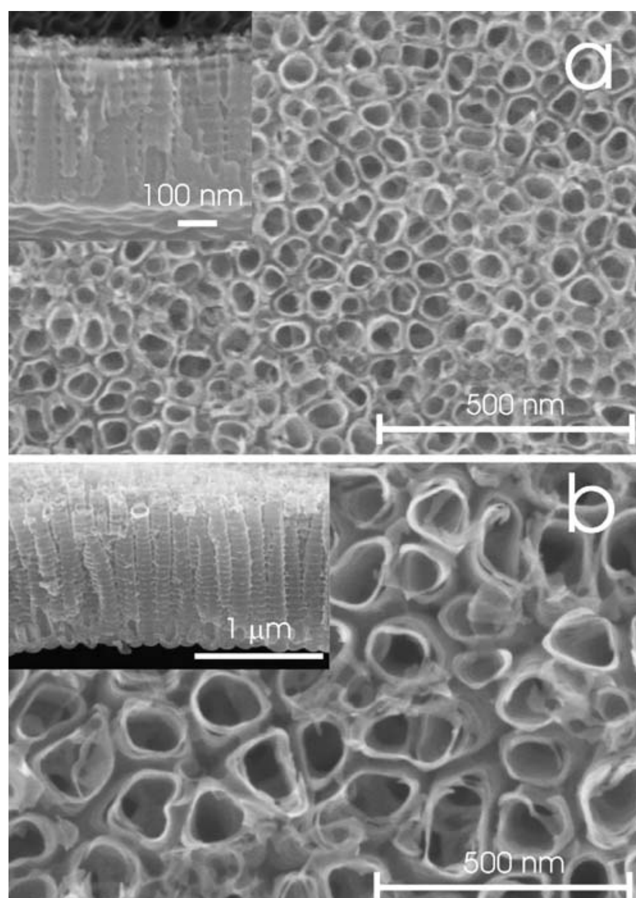

Fig. 1 SEM top view and cross sections for the porous layers formed after anodization in: **a** 1 M NaH_2PO_3+0.3% HF at 10 V and **b** 1 M H_3PO_3+0.5% HF at 20 V

Figure 2b depicts schematically this concept, where an equivalent circuit describing the impedance behavior of the different interfaces is presented. Here, it is also assumed that the complex behavior can be reduced to two parallel resistance–capacitance elements in series with certain frequency dispersion, represented by the α exponent. Solid lines in Fig. 2a show the results from fitting the experimental results according to the model presented in Fig. 2b, whose parameters are summarized in Table 1.

If we look at the results obtained on the amorphous oxide, we can observe that while the capacity of the semiconductor layer increases, that of the Helmholtz layer remains practically constant with a distribution coefficient α of approximately 0.5. Such a coefficient and the constancy of C_H suggest the presence of a diffusion-controlled process that takes place apparently in the base

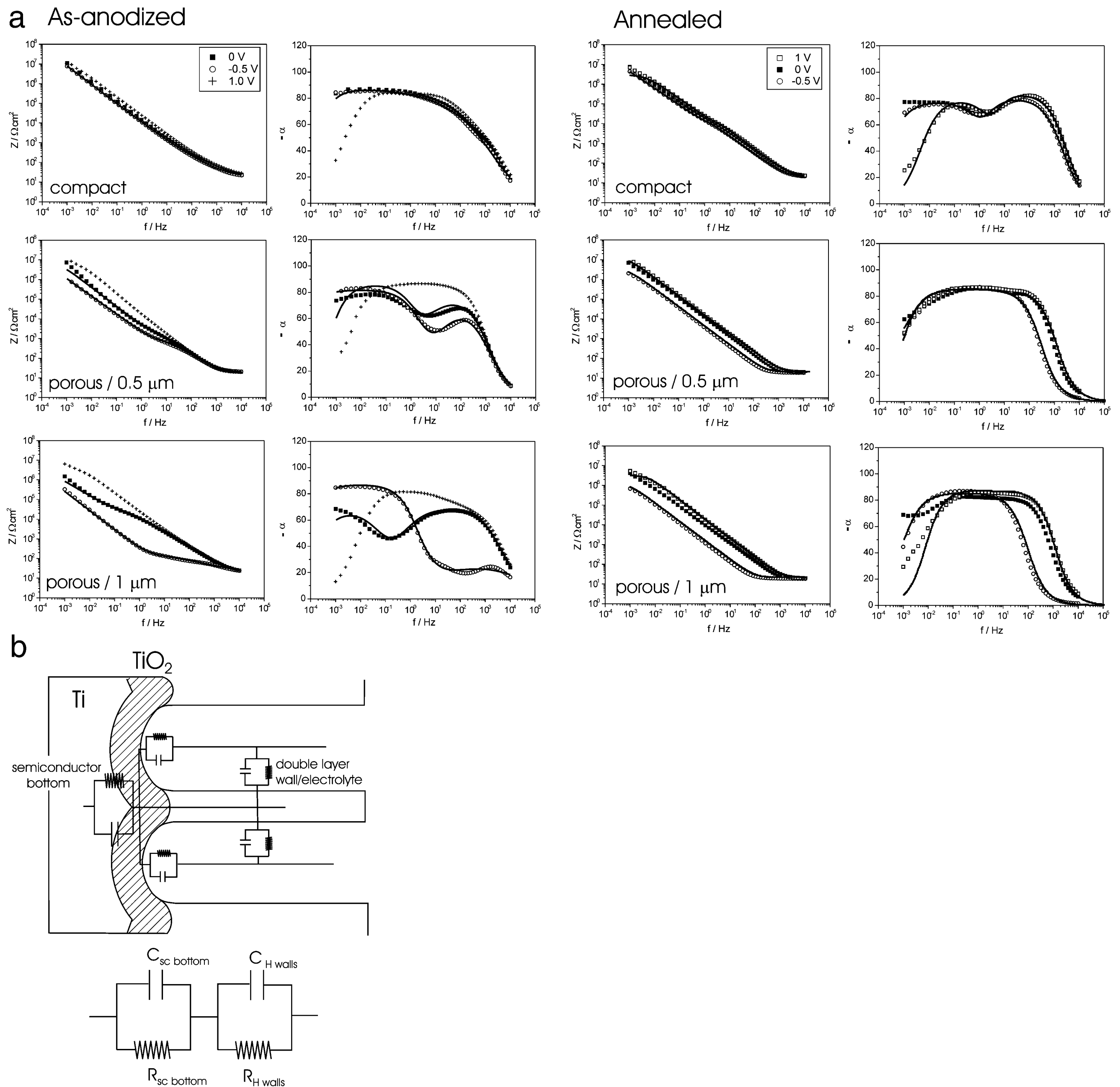

Fig. 2 **a** Impedance spectra taken on as-anodized and annealed compact and porous oxides of 0.5 and 1 μm long tubes at different potentials in acetate buffer solution pH 6. *Symbols*, experimental results; *solid lines*, fitting curves obtained using the model depicted in subpanel b. **b** Equivalent circuit representing the impedance response of the porous TiO_2 layers

of the pores. Then, the increases of oxide capacity can be explained in terms of a shift of the flat band potential toward more positive values as discussed later. This can also be noted by the stronger decay of C_{sc} in the long porous oxide at 0 V due to a larger distance from U_{fb}.

As expected, the oxide annealing introduces substantial modifications in the impedance response of the porous oxides. At $U=-0.5$ V, that is, close to the flat band potential, an increase in both the semiconductor and the Helmholtz capacitance with α of approximately 1 is observed, indicating an interface reaction extended to the whole surface of tubes. It is interesting to note that after driving the potential in the depletion zone of the semiconductor ($U=1$ V), the space charge capacitance takes a similar value for all oxides, whereas the Helmholtz capacitance increases with the area of pores.

The different potential dependences of the Helmholtz capacitance after annealing can be explained in terms of a considerable increase in the electronic conductivity of the oxide tubes as the reduction in the density of traps seems to

Table 1 Circuit parameters obtained after fitting the experimental impedance results showed in Fig. 2a with a two parallel RC circuits connected in series with the electrolyte resistance

	U/V	C_{OX}/μF cm^{-2}	C_H/μF cm^{-2}	R_{OX}/Ω cm^2	R_H/Ω cm^2
Amorphous					
Compact	−0.5	13.2 (0.97)	5.4 (0.56)	58.9×10^6	33.9×10^3
Porous 0.5 μm	−0.5	41.3 (0.91)	8.2 (0.78)	40.6×10^6	6.1×10^2
	0	25.8 (0.96)	6.5 (0.81)	7.1×10^6	1.8×10^3
Porous 1.0 μm	−0.5	398 (0.97)	4.1 (0.41)	4.9×10^6	1.6×10^2
	0	8.4 (0.78)	3.4 (0.77)	4.9×10^6	20.7×10^3
Annealed					
Compact	−0.5	5.5 (0.87)	15.0 (0.96)	20.6×10^6	4.9×10^3
	1.0	3.4 (0.89)	11.5 (1.00)	3.0×10^6	3.8×10^3
Porous 0.5 μm	−0.5	85.0 (0.99)	60 (0.93)	6×10^6	2×10^6
	1.0	10.0 (0.95)	60 (1.00)	18×10^6	1×10^2
Porous 1.0 μm	−0.5	350 (0.98)	150 (0.94)	4.9×10^6	1×10^5
	1.0	6.8 (0.98)	150 (1.00)	3×10^6	2×10^2

In parentheses: α, frequency dispersion coefficient

be a cause for the increase in conductivity, which affects directly the electron mobility [19]. Thus, it would also mean that the constancy of C_H in the amorphous oxides is a consequence of the small reactivity (due to its high resistivity) of the high disordered tubes.

The more disordered structure and the introduction of electrolyte anions into the outermost part of the oxide layer during the anodization lead to the generation of a large amount of oxide defects leading to dissimilar extents of the depletion layer. Therefore, oxide annealing is expected to greatly modify the concentration of defects reducing the density of trapping defects. X-ray photoelectron spectroscopy (XPS) studies performed by Lausmaa et al. [20] and Marino et al. [21] have demonstrated the incorporation of SO_4^{-2} and PO_4^{-3} into the outer layers of the oxide during the anodization, similarly as it occurs in the case of aluminum [22]. The incorporation of anions is expected to depend on the established electric field. Thus, different extent of penetrations and related defects are expected for the oxides obtained under different potential conditions.

Mott–Schottky analysis: enhancement of the interfacial effects in porous oxides

To advance in the understanding of the semiconductor properties of the different oxides, the potential dependence of capacitance was analyzed at different frequencies using the Mott–Schottky theory. This is the most common way to determine the U_{fb} and the donor concentration N in a specific electrochemical system by using the well-known equation valid for the depletion zone of the semiconductor [23]:

$$C_{sc}^{-2} = \left(\frac{2}{\varepsilon\varepsilon_0 eN}\right)(U - U_{fb} - kT/e) \qquad (1)$$

where C_{sc} represents the differential capacitance of the space charge layer. Thus, the flat band potential is given by the extrapolation to C^{-2}=0 whereas N can be calculated from the slope of C^{-2} vs U plots.

The existence of a high concentration of multiple donor levels in the band gap can promote an indirect tunneling of electrons through the semiconductor layer, resulting in a variation of the slope of Eq. (1) with the frequency. This frequency dependence is determined by the distribution of relaxation times for the electron emission to the conduction band, which in turn depends on the position of the states relatively to that. Thus, at a sufficient low frequency, the response of a large fraction of the frequency-dependent donors is expected [24]. In addition, the influence of the Helmholtz capacitance is avoided (cf. Fig. 2a).

Figure 3 presents a comparison of the Mott–Schottky plots obtained on as-anodized and annealed samples at different frequencies. It can be observed that in all cases, the curves show the presence of a change of slope (crossover) that becomes more marked after annealing and which can be associated with the ionization of band states.

Regarding the as-anodized compact and porous oxides, one can observe that here, a wider frequency dispersion than after annealing seems to be present. Then, flat band potentials U_{fb}=−0.8 V and U_{fb}=−0.75 V for the compact and porous layer, respectively, could be estimated at f= 3 Hz. In spite of the proximity of the flat band potentials, some differences can be noted, however, in the potential dependence of the slope, suggesting a higher concentration of energy states near the conduction band of the compact oxide, which in turn is related to a more disordered oxide structure. This is also reflected in the noticeable increase of the slope after annealing in the compact oxide, which contrasts practically with the absence of changes in the porous layer. In both cases, the annealing leads to a narrower frequency-dispersion, i.e., a sharper distribution of the relaxation times of ionization. Although similar diagrams are observed for the compact and porous oxides after annealing, lower values are observed for the latter.

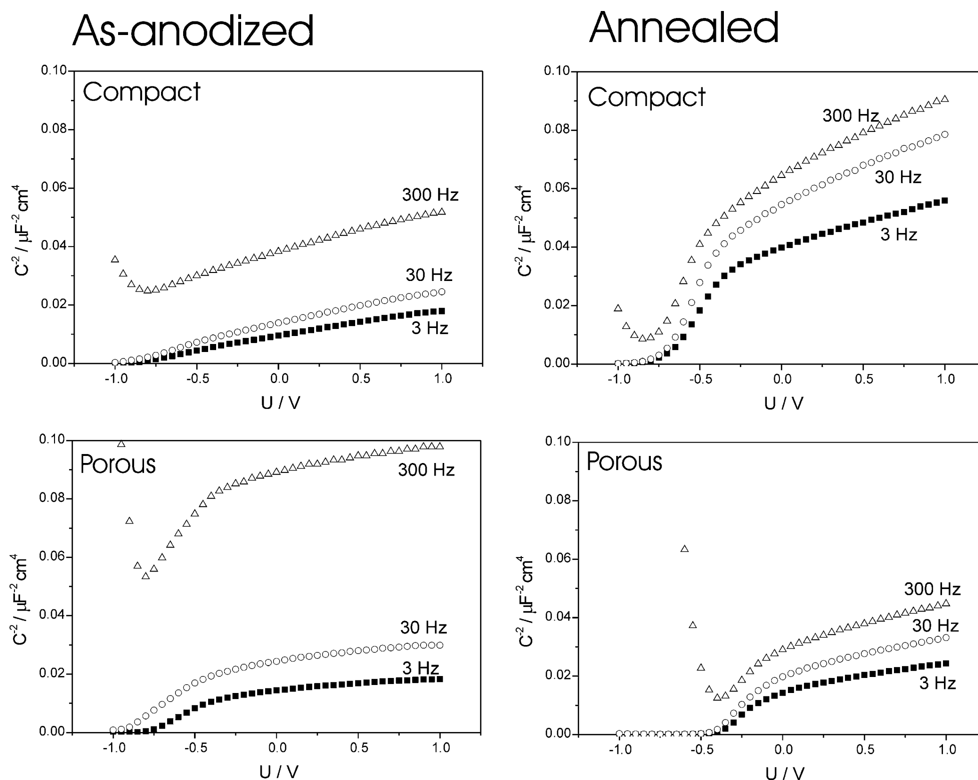

Fig. 3 Mott–Schottky plots obtained before and after annealed on compact oxide and porous layers of 1-μm-long tubes in acetate buffer solution of pH 6. f=300 to 3 Hz

This result cannot simply be explained considering a larger surface area of the porous layer with the semiconductor behavior of the compact oxide. By considering that $1/C_{geom}{}^2=(A_{geom}/A_{porous})^2\ (1/C_{real}{}^2)$, a ratio of ($A_{porous}/A_{geom}$) approximately 1.5 is obtained (using the capacitance values at the crossover). This value appears unrealistic as a factor of 20 can be estimated from SEM images. Furthermore, the marked difference of the flat band potentials of the annealed oxides (U_{fb}=−0.725 V for the compact and U_{fb}=−0.33 V for the porous layer) cannot be explained in terms of a change in surface area (cf. Fig. 4). A significant shift of the flat band potential is also observed comparing the porous oxide before and after annealing. Then, the fact that the shape of the Mott–Schottky curve remains practically without changes suggests that this potential shift is rather related with a shift of the Fermi level of the oxide caused by: (1) the presence of a second more conductive oxide film with a different Fermi level or (2) the variation of the potential drop at the oxide/electrolyte interface as a consequence of a change in the surface chemistry.

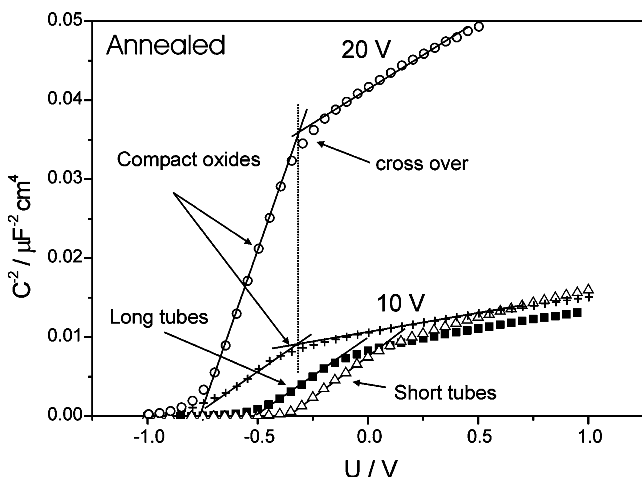

Fig. 4 Comparative Mott–Schottky plots obtained on annealed compact and porous layers in acetate buffer solution of pH 6 and at f=3 Hz

Values of $N=4.19\times10^{19}$ cm^{-3} and an apparent $N^*=1.63\times10^{20}$ cm^{-3} (referred to the geometrical area) for the annealed compact and porous layer, respectively, were estimated from the first linear part of the C^{-2} vs U plots by using Eq. (1). Thus, the idea of interpreting the behavior of the porous oxide as a simple extension of the surface area of the compact oxide does not seem to be in line with the expected increase of the donor concentration. In fact, if this was the case, the density of the donor would be given by the relation: $N_{porous}=(A_{geom}/A_{porous})^2N_{geom}$. After an estimate of the area of tubes from the SEM pictures, a value of $N_{porous}=9.5\times10^{16}$ cm^{-3} is obtained, which appears to be quite low for anodic oxides. Although the values reported for the donor concentration vary markedly according to the preparation conditions, they are typically within the range 10^{19}–10^{20} cm^{-3} [25–27]. Therefore, an explanation considering a very low donor density in the pore walls seems rather unlikely.

A more realistic hypothesis for explaining these results assumes a highly doped tube structure, in such an extent

that a larger space charge layer will be built at the base of the pores whereon the density of defects is expected to be similar to the compact oxide. Therefore, one could model the porous layer as a duplex oxide constituted by highly conducting tubes placed on a base oxide layer, as already suggested in the discussion of the impedance spectra.

The presence of two regions in the Mott–Schottky plots is another matter of discussion and is a characteristic feature observed in TiO_2 layers. The crossover was already observed by Van de Krol et al. [28] on studying e-beam deposited TiO_2 films on conducting glass. They explained this fact in terms of a limitation of the space charge layer growth by the film thickness. However, this explanation does not seem to be convincing in our case. The depletion layer length of a semiconductor can be estimated by:

$$L_D = \left(\frac{2\varepsilon\varepsilon_0}{eN_D}\right)^{1/2}(U - U_{fb} - kT/e)^{1/2} \qquad (2)$$

where ε is the dielectric constant of TiO_2, assumed equal to 42. According to Eq. (2), a length of 7 nm for the space charge layer is estimated at the crossover potential for the compact layer formed at 20 V, with a thickness of ca. 50 nm. Moreover, practically the same crossover potential is observed for an oxide of 25 nm thicknesses (cf. Fig. 4). Therefore, different slopes in the low band-bending regions are attributed to a dependence of the concentration of defects on the formation potential [29].

Other authors [29, 30], however, considered the existence of multiple donor levels that are successively ionized with the potential increase for explaining the presence of a crossover. This would lead to a continuous change of the Mott–Schottky slope with potential, which can be resolved by applying the modified Mott–Schottky equation proposed by Dean and Stimming [31]. This analysis predicts a continuous increase of the donor concentration up to a constant value at (U−U_{fb}) of approximately 1 V for anodic amorphous TiO_2 [29], pointing out the presence of a donor band below the conduction band. The present findings show that crossover occurs for compact annealed and nonannealed films and for tubular annealed and non-annealed films. This clearly supports the idea of an intrinsic TiO_2 electronic state model rather than a geometrical effect.

The influence of pH

To investigate the interfacial effects of the oxide on the semiconductor properties, the Mott–Schottky analysis was performed on annealed oxides in buffer solutions of different pH's (Fig. 5). It can be observed that the low band-bending parts of the curves shift toward more negative values with pH increase. This potential shift reflects the change of the potential drop at the double layer as a consequence of the acid–base reaction of the surface–

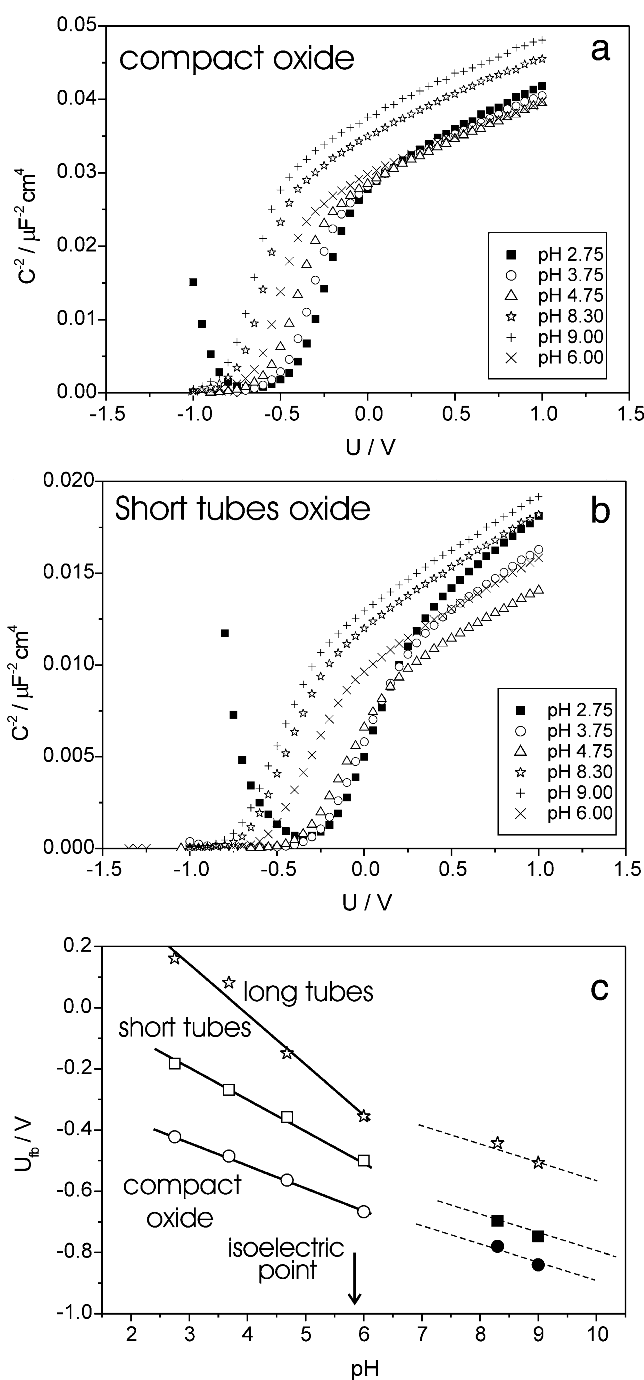

Fig. 5 pH dependence of the Mott–Schottky plots obtained on annealed **a** compact and **b** porous (with 1-µm-long tubes) oxides. **c** pH dependence of the flat band potential for the different oxides obtained by extrapolation of the low band-bending parts to C^{-2}=0

OH groups. Thus, in the absence of surface states and adsorbed ions, the following pH dependence of the flat band potential is expected:

$$U_{fb} = U_{fb,iep} - 2.3\,kT\left(\mathrm{pH} - \mathrm{pH}_{iep}\right) \qquad (3)$$

where $U_{fb,iep}$ and pH_{iep} are the flat band potential and the pH at the isoelectric point, respectively, which was recently

reported to be 5.8 for anatase [31]. Two zones can be clearly distinguished at both sides of the isoelectric point, where a marked increase of the slope of the U_{fb} vs pH plots is observed for the porous films. For instance, the compact oxide shows a slope of 75 mV/pH (Fig. 5c), which is higher than 59 mV/pH as predicted by Eq. (3) for an ideal case. This fact indicates some lack of ideality in the surface chemistry of the oxide. This slope deviates even more from the ideal value for the porous oxides, with values of 105 mV/pH and 166 mV/pH for the 0.5 and 1 μm long tubes, respectively, indicating a strong influence of the surface chemistry. This result suggests that the extended area of the high defective oxide tubes generates a larger amount of surface states with a consequent stronger Fermi level pinning effect on the base of pores. This in turn is related to the higher surface capacity shown by the porous oxides in the annealed form (Table 1).

The fact that different slopes are observed around the isoelectric point may be related to the nature of the surface states. In fact, it was suggested that the formation of surface states is related on incomplete coordination of surface Ti atoms [32], which seems to be favored at pH < pH_{iep}.

The change of solution pH also affects, but in a lesser extent, the concentration of donors, as can be inferred from some pH dependence of the slopes of the Mott–Schottky plots. This effect is more pronounced in the high band-bending zone and even more in the case of the short tubes oxide (cf. Fig. 5b). This effect cannot be associated with the reductive effects of the hydrogen intercalation, which is observed at potential more negative than the flat band condition with a consequent marked increase of the donor concentration [18, 32]. Furthermore, the results presented in Fig. 5 were obtained with a potential scan starting from the anodic limit toward cathodic potentials. Therefore, it is clear that the effects of pH are rather related to modifications of the surface chemistry.

Model

The impedance behavior of the porous structures can be interpreted considering a duplex oxide structure where the wall of the oxide tubes present a higher donor concentration with a consequent higher electronic conductivity than the underlying layer, whose behavior can be considered similar to the compact oxide (Fig. 2b). According to this model and accepting that the system is under electronic equilibrium, the introduction of the pore walls with a higher donor concentration will shift the energy levels of the compact layer toward higher energies (cf. Fig. 6). This, in turn, is reflected by a positive shift of the observed flat band potential. The total capacitance of the oxide will be given by:

$$\frac{1}{C_{ox}} = \frac{1}{C_{SC(bottom)}} + \frac{1}{C_{SC(walls)}} \tag{4}$$

Taking into account that $C_{sc} \propto \sqrt{N_D}$ in the depletion region and that $N_{walls} >> N_{bottom}$, the observed capacity response will be dominated by the underlying oxide, i.e., $C_{ox} \approx C_{sc(bottom)}$. Due to the high conductivity of the walls, the nanotubes can be regarded as an electronic conductor connecting the base semiconductor with the double layer in the solution side. Therefore, the observed response corresponds to that of the bottom oxide, whereas the influence of the oxide tubes can be centralized in the shift of the Fermi niveau of the underlying bottom oxide together with the enhanced surface chemistry effects.

The annealing process causes a decrease of the concentration of defects. As a consequence, the flat band potential shifts toward more positive potentials. Therefore, the different Fermi level shifts in the base and walls conduct to a more marked effect in the case of porous oxides (cf. Fig. 3).

The effects of the presence of a porous structure on the pH dependence of the flat band potential can also be related

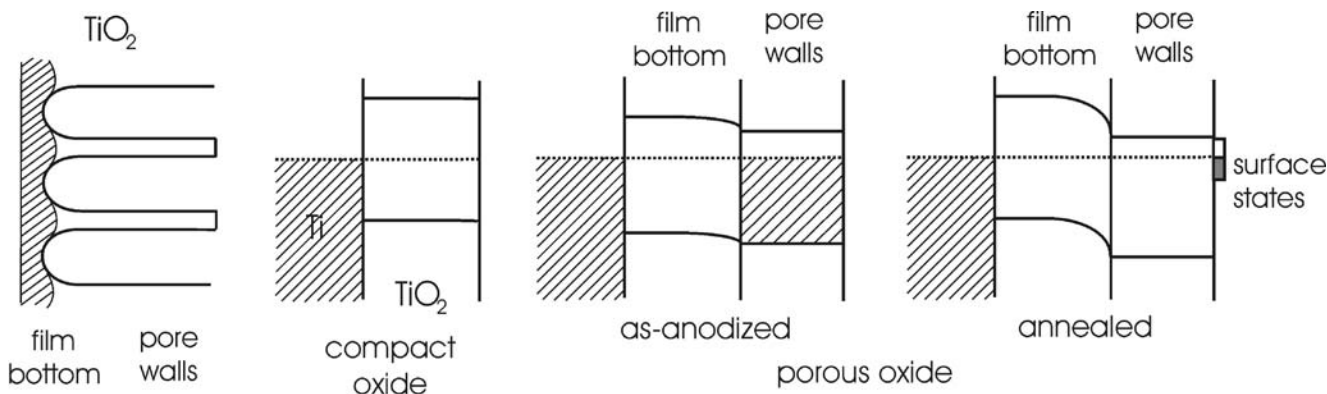

Fig. 6 Schematic representation of the porous oxide structure with the corresponding changes of energy levels of the compact oxide before and after the contact with the as-anodized and annealed pore walls

to the double semiconductor structure. Here, it is expected that the shift of the Fermi level of the compact oxide will be controlled by the surface chemistry of the pore walls. Thus, the noticeable potential shift at pH<6 in the porous oxide (cf. Fig. 5c) can be explained in terms of the acid–base reactions of the –OH groups on the surface of the pore walls and the fact that the potential drop “seen” by the underlying oxide is given by:

$$\Delta\varphi_{\mathrm{ox-el}} = \frac{\Delta q A_{\mathrm{pores}}}{C A_{\mathrm{bottom}}} \qquad (5)$$

as part of the surface charge generated in the pore walls must be compensated in the bottom oxide. The presence of these groups would also conduct to the formation of surface states, whose charging brings about a pinning of the Fermi level. However, more work is necessary to throw light on this matter.

Conclusions

According with the results of the impedance study of the semiconductor properties, there is evidence for different electronic structures of the walls of pores and the underlying oxide. Thus, their semiconductor behavior can be well explained considering a high conductive structure of the wall of oxide tubes in electronic equilibrium with a compact oxide in the bottom. In this structure, the surface chemistry of the tubes introduces considerable changes in the semiconductor behavior of the compact layer such as the shift of the flat band potential.

Acknowledgment The authors wish to acknowledge the financial support from the Deutsche Forschungsgemeinschaft (DFG).

References

1. Grätzel M (2003) J Photochem Photobiol C 4:145
2. Dyer CK, Leach JSL (1978) J Electrochem Soc 125:1032
3. Schultze JW, Lohrengel MM, Ross D (1983) Electrochim Acta 28:973
4. Schmuki P (2002) J Solid State Electrochem 6:145
5. Akbar SA, Younkman LK (1997) J Electrochem Soc 144:1750
6. Savage NO, Akbar SA, Dutta PK (2001) Sens Actuators B 72:239
7. Birkefeld LD, Azad AM, Akbar SA (1992) J Am Ceram Soc 75:2964
8. Sakthivel S, Kisch H (2003) ChemPhysChem 4:487
9. Sasahi R, Morikawa T, Ohwaki T, Aoki A, Taga Y (2001) Science 293:269
10. O’Regan B, Grätzel M (1991) Nature 353:737
11. Grätzel M (2001) Nature 414:338
12. Ghicov A, Tsuchiya H, Macak JM, Schmuki P (2005) Electrochem Commun 7:505
13. Tsuchiya H, Macak JM, Taveira L, Balaur E, Ghicov A, Sirotna K, Schmuki P (2005) Electrochem Commun 7:576
14. Macak JM, Tsuchiya H, Schmuki P (2005) Angew Chem Int Ed 44:2100
15. Macak JM, Sirotna K, Schmuki P (2005) Electrochim Acta 50:3679
16. Law M, Greene L, Johnson JC, Saykally R, Yang P (2005) Nat Matters 4:455
17. Ghicov A, Tsuchiya H, Macak JM, Schmuki P (2005) Electrochem Commun 7:505
18. Boschloo GK, Goossens A, Schoonman J (1997) J Electrochem Soc 144:1311
19. Eppler AM, Ballard IM, Nelson J (2002) Phys E 14:197
20. Lausmaa J, Kasemo B, Mattsson H, Odelius H (1990) Appl Surf Sci 45:189
21. Marino CEB, Nascente PAP, Biaggio SR, Rocha-Fihlo RC, Bocchi N (2004) Thin Solid Films 468:109
22. Thompson GE (1997) Thin Solid Films 297:192
23. Sato N (1998) Electrochemistry at metal and semiconductor electrodes. Elsevier
24. Di Quarto F, La Mantia F, Santamaría M (2005) Electrochim Acta 50:5090
25. Oliva FY, Avalle LB, Santos E, Cámara OR (2002) J Photochem Photobiol A 146:175
26. Dolata M, Kedzierzawski P, Augustynski J (1996) Electrochem Acta 41:1287
27. Simons W, Pauwels L, Hubin A (2002) Electrochim Acta 47:2169
28. Van de Krol R, Groossens A, Schoonman J (1997) J Electrochem Soc 144:1723
29. Lee E-J, Pyun S-I (1992) J Appl Electrochem 22:156
30. Simons W, Hubin A, Vereecken J (1999) Electrochim Acta 44:4373
31. Dean MH, Stimming U (1989) Corros Sci 29:199
32. Boschloo GK, Goossens A (1996) J Phys Chem 100:19489